Amyloid-β regulates gap junction protein connexin 43 trafficking in cultured primary astrocytes

Received for publication, April 1, 2020, and in revised form, August 6, 2020 Published, Papers in Press, August 31, 2020, DOI 10.1074/jbc.RA120.013705

Mahua Maulik*, Lakshmy Vasan, Abhishek Bose, Saikat Dutta Chowdhury, Neelanjana Sengupta, and Jayasri Das Sarma

From the Department of Biological Sciences, Indian Institute of Science Education and Research Kolkata, Mohanpur, West Bengal, India

Edited by Phyllis I. Hanson

Altered expression and function of astroglial gap junction protein connexin 43 (Cx43) has increasingly been associated to neurotoxicity in Alzheimer disease (AD). Although earlier studies have examined the effect of increased β-amyloid (Aβ) on Cx43 expression and function leading to neuronal damage, underlying mechanisms by which Aβ modulates Cx43 in astrocytes remain elusive. Here, using mouse primary astrocyte cultures, we have examined the cellular processes by which Aβ can alter Cx43 gap junctions. We show that $A\beta_{25\text{-}35}$ impairs functional gap junction coupling yet increases hemichannel activity. Interestingly, $A\beta_{25\text{-}35}$ increased the intracellular pool of Cx43 with a parallel decrease in gap junction assembly at the surface. Intracellular Cx43 was found to be partly retained in the endoplasmic reticulum-associated cell compartments. However, forward trafficking of the newly synthesized Cx43 that already reached the Golgi was not affected in $A\beta_{25\text{-}35}$-exposed astrocytes. Supporting this, treatment with 4-phenylbutyrate, a well-known chemical chaperone that improves trafficking of several transmembrane proteins, restored Aβ-induced impaired gap junction coupling between astrocytes. We further show that interruption of Cx43 endocytosis in $A\beta_{25\text{-}35}$-exposed astrocytes resulted in their retention at the cell surface in the form of functional gap junctions indicating that $A\beta_{25\text{-}35}$ causes rapid internalization of Cx43 gap junctions. Additionally, *in silico* molecular docking suggests that Aβ can bind favorably to Cx43. Our study thus provides novel insights into the cellular mechanisms by which Aβ modulates Cx43 function in astrocytes, the basic understanding of which is vital for the development of alternative therapeutic strategy targeting connexin channels in AD.

Connexin 43 (Cx43) is a predominant gap junction protein that underlies astroglial networks essential for maintaining brain homeostasis (1–6). Gap junctions are arrays of a few tens to thousands of cell-to-cell channels, termed as gap junction channels that allow direct intercellular exchange of small molecules such as ions (Ca^{+2}, K^+, Na^+), amino acids (glutamate), second messengers (ATP, cAMP, and inositol 1,4,5-trisphosphate) and metabolites (GSH, glucose) up to approximately 1 kDa in size (7, 8). A single gap junction channel comprises two opposing channels, called hemichannels or connexons, formed by oligomerization of six connexin proteins. Under normal conditions, hemichannels exhibit a low probability of opening and have been proposed to mediate physiologic release of gliotransmitters in the extracellular medium (9, 10).

Accumulating evidence suggests that altered functioning of gap junctions and hemichannels could be related to the onset and progression of homeostatic imbalances observed in various neurodegenerative diseases (11, 12). In fact, loss of astrocytic gap junctions in mice has been shown to cause profound neurological phenotypes including widespread dysmyelination and hippocampal CA1 vacuolation (13). In this context, several recent studies have revealed an association between astroglial connexins and the neurodegenerative phenotype observed in Alzheimer's disease (AD), the most prevalent cause of dementia largely affecting the elderly population (14, 15). Accumulation of β-amyloid (Aβ) peptides and reactive astrogliosis are among the pathological features that characterize all AD brains with Aβ peptides widely believed to drive AD neuropathology (16, 17). Although Aβ neurotoxicity involves activation of *N*-methyl-D-aspartate receptors, sustained elevations of Ca^{2+}, mitochondrial dysfunction, oxidative stress, and immune activation (18), complete understanding of the underlying mechanisms associated with AD pathology remain elusive.

Interestingly, several recent studies indicate that astroglial Cx43 channel functions, both gap junctions as well as hemichannels, are modified in AD. Studies in post-mortem human AD brains and mouse models of AD have shown increased immunoreactivity of Cx43 around Aβ plaques (19–21). In cultured rat astrocytes, $A\beta_{1\text{-}40}$ treatment was reported to impair gap junction communication (22). However, the extent of gap junction coupling in astrocytic networks in brain slices of AD mouse models was found to be either maintained or reduced depending on the brain area and age of the animal (21, 23). Recently, it was shown that treatment with $A\beta_{25\text{-}35}$ increased Cx43 hemichannel activity in astrocytes releasing ATP and glutamate subsequently leading to neuronal damage (24). Supporting this, inhibition of glial hemichannels prevented the inflammatory profile evoked by Aβ in astrocytes and reduced neuronal damage in hippocampal slices exposed to Aβ as well as in AD mouse model (25, 26). Furthermore, astroglial targeted connexin 43 knockout in a mouse model of AD lessened neuronal damages and improved cognitive function (21, 27).

This article contains supporting information.

* For correspondence: Mahua Maulik, mahua@iiserkol.ac.in.

Present address for Lakshmy Vasan: Dept. of Laboratory Medicine and Pathobiology, University of Toronto, Toronto, Ontario, Canada.

Altogether, these earlier studies suggest that Aβ alters Cx43 function in astrocytes leading to neurotoxicity and that Cx43 could be a potential therapeutic target for AD. However, the underlying mechanisms by which Aβ modulates Cx43 function in astrocytes remain largely unknown.

In the present study, we have examined the cellular mechanisms by which $A\beta_{25\text{-}35}$, the shortest neurotoxic peptide form of Aβ (28), can modulate Cx43 channels in mouse primary cultured astrocytes. $A\beta_{25\text{-}35}$ previously considered to be a mere synthetic peptide, is physiologically produced and present in senile plaques and degenerating hippocampal neurons in AD brains (29). Numerous studies performed *in vitro* as well as *in vivo* using intra-cerebroventricular injection of $A\beta_{25\text{-}35}$ in experimental rats and mice showed that this peptide can recapitulate many of the neuropathological changes related to AD establishing $A\beta_{25–35}$ to be a convenient model to evaluate the potential toxicity involved in AD (30). We show that $A\beta_{25\text{-}35}$ impairs functional gap junction coupling but increases hemichannel activity in mouse primary astrocytes. Interestingly, $A\beta_{25\text{-}35}$ treatment increased intracellular Cx43 expression that was partly retained in the endoplasmic reticulum (ER) and ER Golgi intermediate compartments (ERGIC). Furthermore, we show that $A\beta_{25\text{-}35}$ increased internalization of Cx43 from the cell surface inhibiting functional gap junction intercellular communication between astrocytes. Taken together, our findings reveal that Aβ affects intracellular trafficking of Cx43 impacting the formation and maintenance of gap junction channels at the cell surface.

Results

Aβ differentially regulates functional gap junction and hemichannel activity in mouse primary astrocytes

To determine the effect of Aβ on gap junctions, mouse primary astrocytes were treated with 10 μM $A\beta_{25\text{-}35}$ for 24, 48, and 72 h and functional gap junction communication was evaluated by scrape loading and dye transfer assay with a gap junction permeable Lucifer yellow dye (Fig. 1, *A–E*). Control astrocytes showed significant dye spread from the scrape loading line (Fig. 1*A*) and reached 328.6 ± 19.38 μM after 8 min (Fig. 1*E*). By contrast, $A\beta_{25\text{-}35}$-treated astrocytes showed a significant reduction in dye transfer in a time-dependent manner (Fig. 1, *B–D*) with a mean dye travel distance of 66.71 ± 6.87 μM following 72 h exposure to 10 μM $A\beta_{25\text{-}35}$ (Fig. 1*E*). We next evaluated hemichannel activity in control and $A\beta_{25\text{-}35}$-treated mouse primary astrocytes cultures using EtBr (5 μM) uptake assay where EtBr fluorescent signal in the nucleus of GFAP-labeled astrocytes was taken as an index of dye uptake (Fig. 1, *F* and *G*). Although the control astrocytes showed only a faint intensity of EtBr signal, mouse primary astrocytes treated with 10 μM $A\beta_{25\text{-}35}$ for 72 h presented significantly higher intensity of EtBr labeling. In parallel cultures, primary astrocytes treated with the reverse sequence of $A\beta_{25\text{-}35}$, $A\beta_{35\text{-}25}$, did not induce such effects (Fig. S1). Thus, our results suggest that $A\beta_{25\text{-}35}$ significantly impairs functional gap junction communication while increasing hemichannel activity in mouse primary astrocyte cultures.

Aβ increases intracellular Cx43 expression without altering its steady-state levels in mouse astrocytes

To determine whether the altered functioning of gap junctions and hemichannels was because of a change in steady-state Cx43 levels, we examined Cx43 mRNA and total protein levels. Our quantitative PCR analysis showed no significant alterations in Cx43 mRNA levels in mouse primary astrocytes treated with 10 μM $A\beta_{25\text{-}35}$ for 24, 48, and 72 h compared with control astrocytes (Fig. 2*A*). Consistent with the mRNA levels, Cx43 total protein expression also did not reveal any significant alterations in mouse astrocyte cultures subjected to 10 μM $A\beta_{25\text{-}35}$ for 24, 48, and 72 h compared with control astrocytes (Fig. 2*B*). Antibody directed against Cx43 detected three bands at around 43 kDa, representing a faster migrating nonphosphorylated form (P0) and two slower migrating phosphorylated forms (P1, P2) (31). No significant difference was noted in the steady-state levels of the phospho-bands in $A\beta_{25\text{-}35}$-treated *versus* control astrocytes. Thus, Cx43 steady-state levels were not found to be significantly altered in mouse primary astrocyte cultures treated with $A\beta_{25\text{-}35}$. To examine if the observed changes in functional gap junction communication and hemichannel activity was because of changes in cellular distribution of Cx43, we determined the cellular expression pattern of Cx43 by immnolabeling studies (Fig. 2, *C* and *D*). Although control astrocytes showed mostly an organized distribution with lined up Cx43 puncta typically representing the cell-cell junctions (Fig. 2*C*), mouse astrocytes treated with 10 μM $A\beta_{25\text{-}35}$ for 72 h showed Cx43 labeling scattered throughout the cell cytoplasm (Fig. 2*D*). Interestingly, in many places Cx43 labeling was also found to be accumulated near the perinuclear region suggesting an increase in intracellular Cx43 levels (Fig. 2*D*, *arrowheads*). Additionally, astrocytes showed heterogeneous Cx43 labeling with punctate structures of varied sizes. Although larger puncta might correspond to gap junction plaques at the cell–cell interface, smaller puncta might represent intracellular Cx43 to be sorted to the plasma membrane or small junctions internalized and targeted for degradation. The quantification of Cx43 punctate areas revealed significant difference between control and $A\beta_{25\text{-}35}$-treated astrocytes with $A\beta_{25\text{-}35}$-treated cultures showing a lower frequency of large Cx43 puncta >1 μm^2 in size (Fig. 2*E*).

Effect of Aβ on Cx43 gap junction assembly in mouse primary astrocytes

It is well-established that gap junction plaques are resistant to 1% Triton X-100 at 4 °C, whereas monomers and lower oligomers of Cx43 are mostly solubilized under such conditions (32, 33). To understand Cx43 assembly into gap junctions, membrane-enriched fractions from control and $A\beta_{25\text{-}35}$-treated mouse astrocytes were subjected to 1% Triton X-100 at 4 °C in a detergent solubility assay, separated into Triton X-100–soluble and –insoluble fractions and analyzed by immunoblotting for Cx43 antibody (Fig. 3*A*). Our results show that Cx43 levels are decreased in the Triton X-100–insoluble fractions with a concomitant increase in Triton X-100–soluble fractions of $A\beta_{25\text{-}35}$-treated cultures compared with control astrocytes consistent with reduced functional gap junction

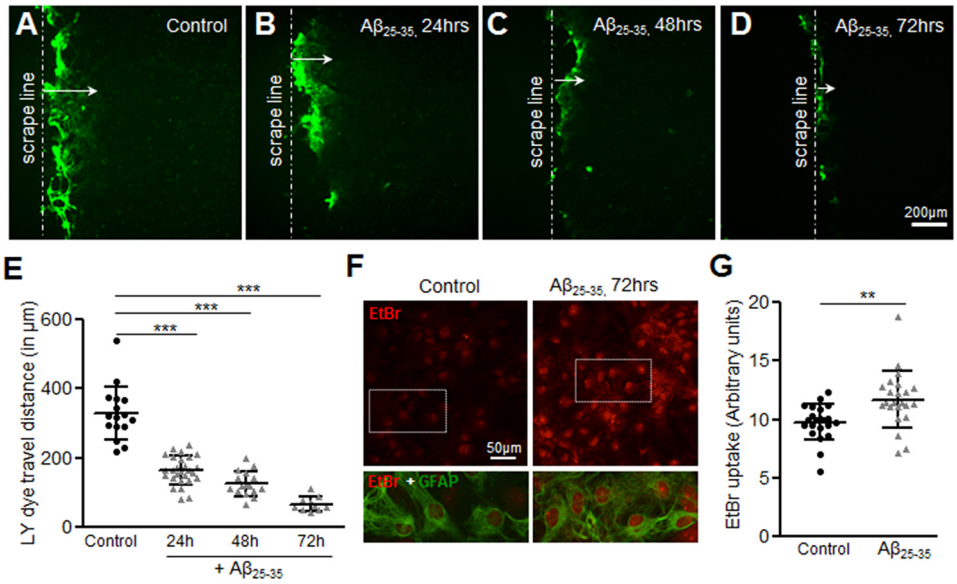

Figure 1. Aβ$_{25-35}$ differentially regulates functional gap junction coupling and hemichannel activity in mouse primary astrocytes. *A–D*, representative photomicrographs showing the Lucifer yellow dye spread from the scrape loading line (*arrow*, *A*) in mouse primary astrocyte cultures under control conditions (*A*) or treated with 10 μM Aβ$_{25-35}$ for 24 (*B*), 48 (*C*), and 72 h (*D*). Note the decrease in dye travel distance in Aβ$_{25-35}$-treated astrocytes with the increasing time compared with control astrocytes. *E*, scatter plot depicting a significant decrease in Lucifer yellow dye spread representing impaired functional gap junction coupling between mouse primary astrocytes upon treatment with 10 μM Aβ$_{25-35}$ in a time-dependent manner compared with control astrocytes. *F*, representative images illustrating EtBr dye uptake (*red* nucleus staining) in control *versus* Aβ$_{25-35}$-treated (10 μM, 72 h) astrocytes. Although the control cultures show only a low basal EtBr uptake, Aβ$_{25-35}$-treated cultures show increased EtBr signal in the nuclei of GFAP-positive astrocytes. *G*, scatter plot depicting the relative fluorescence intensities of the nuclei in control *versus* Aβ$_{25-35}$-treated astrocytes (10 μM, 72 h) following 10 min exposure to EtBr. *Error bars* denote the mean ± S.D. of five to 10 fields each from three independent experiments. **, $p < 0.01$ and ***, $p < 0.0001$ compared with control.

communication in Aβ$_{25-35}$-treated astrocytes (Fig. 3*A*). Furthermore, upon *in situ* Triton X-100 extractions, control astrocytes retained Cx43 puncta mostly at the cell–cell junctions, representing gap junctions (Fig. 3*B*, *arrowheads*). Interestingly, *in situ* Triton X-100 extraction in Aβ$_{25-35}$-treated astrocytes confirmed that the majority of the Triton X-100–insoluble Cx43 puncta corresponded to the intracellular pool (Fig. 3*C*, *arrows*), with occasional plasma membrane labeling (Fig. 3*C*). Thus, our results indicate that mouse primary astrocytes exposed to 10 μM Aβ$_{25-35}$ for 72 h exhibit reduced gap junction labeling with a concomitant increase in intracellular Cx43 localization that may correspond to either internalized gap junctions or small aggregates of Cx43 that fail to traffic to the plasma membrane.

Aβ treatment causes Cx43 retention in ER/ERGIC of mouse primary astrocytes

To further understand where the intracellular Cx43 pool may be localized in Aβ-treated astrocytes, we performed double immunolabeling with anti-Cx43 and well established markers of the ER (calnexin; Fig. 4, *A–I*) or ER Golgi intermediate compartments (ERGIC, β-COP; Fig. 5, *A–I*) followed by confocal microscopy. Consistent with our previous findings, control astrocytes showed distinct organization of Cx43 puncta mostly away from the nucleus (Figs. 4, *A–C* and 5, *A–C, small arrows*) without much co-localization with either calnexin (Fig. 4, *A–C*) or β-COP (Fig. 5, *A–C*). In contrast, mouse primary astrocytes subjected to 10 μM Aβ$_{25-35}$ for 72 h showed a reticular staining pattern in the perinuclear region that co-localized mostly with calnexin (Fig. 4, *D–F*, *arrowheads*) and also with β-COP (Fig. 5, *D–F*, *arrowheads*). The number of points showing colocalization of Cx43 puncta with either calnexin (Fig. 4, *G–I*) or β-COP (Fig. 5, *G–I*) was found to be significantly higher in Aβ-treated astrocytes compared with control cultures. Thus, our results show that a portion of the intracellular Cx43 was retained in the ER/ERGIC in mouse primary astrocytes exposed to 10 μM Aβ$_{25-35}$ for 72 h compared with control astrocytes.

4-Phenylbutyrate restores functional gap junction communication in Aβ-treated mouse primary astrocytes

Given that Aβ$_{25-35}$ treatment increased localization of Cx43 in the ER/ERGIC cellular compartments, we reasoned that Aβ might impair proper folding and oligomerization of Cx43, which is a pre-requisite for trafficking of Cx43 to the cell surface. In this context, 4-phenylbutyrate (4-PBA), a well-known histone deacetylase inhibitor, has been reported to restore proper trafficking of several mutant and misfolded transmembrane proteins including connexins to the cell surface (34–36). Hence, we subjected control and Aβ$_{25-35}$-treated (10 μM, 72 h) mouse astrocyte cultures to 5 mM 4-PBA for 24 h. Our immunolabeling studies with anti-Cx43 antibody (Fig. 6, *A–D*) showed a more organized distribution of Cx43 as short lines of Cx43 puncta typically representing gap junctions following 4-PBA treatment in Aβ$_{25-35}$-treated astrocytes (Fig. 6*D*). Astrocytes exposed to Aβ$_{25-35}$ alone exhibited Cx43 labeling scattered throughout the cytoplasm as shown earlier (Fig. 6*C*). Supporting this, Lucifer yellow dye transfer assays, clearly showed that 4-PBA restored functional gap junction communication in Aβ$_{25-35}$-treated astrocyte cultures similar to control astrocytes

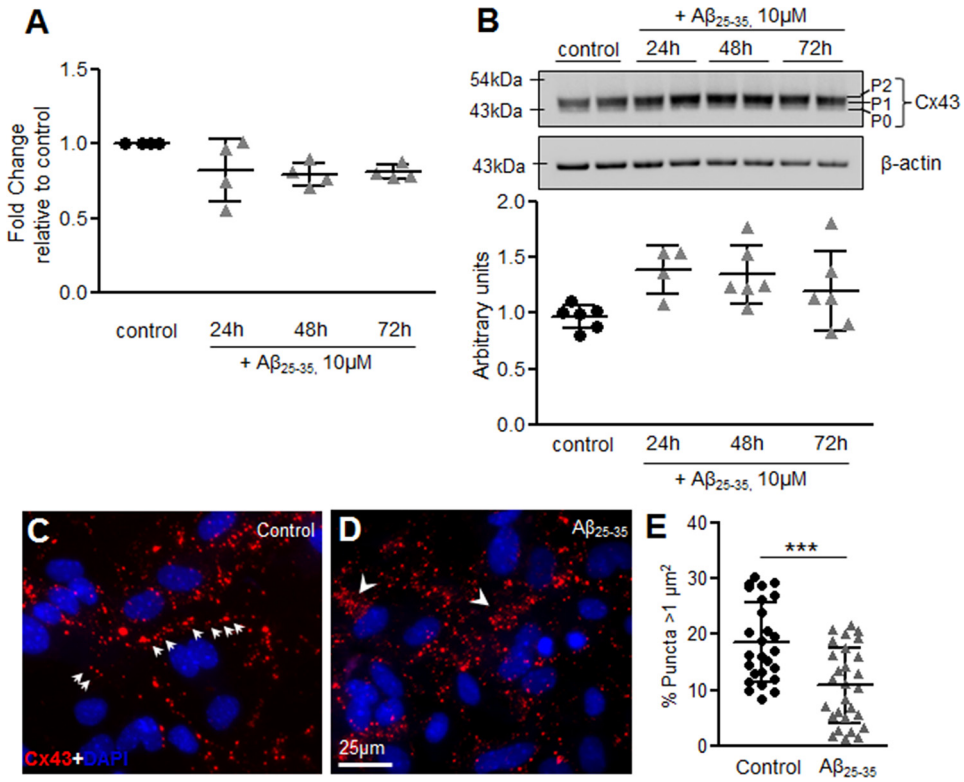

Figure 2. Aβ$_{25-35}$ treatment increases intracellular Cx43 levels without affecting Cx43 steady state levels. *A,* scatter plot showing no significant difference in fold-change of Cx43 mRNA levels in mouse primary astrocytes treated with 10 μM Aβ$_{25-35}$ for 24, 48 and 72 h compared with control astrocytes. Values represent mean ± S.D. from four independent experiments. *B,* representative immunoblot and scatter plot showing Cx43 protein levels in control *versus* Aβ$_{25-35}$ treated (10 μM) astrocytes for the mentioned time points. Cx43 phosphorylated (*P1*, *P2*) and nonphosphorylated (*P0*) forms are indicated on the *right* of the representative image of the blot probed with anti-Cx43 antibody. Total levels of Cx43 are normalized to β-actin levels detected in each lane. Values represent mean ± S.D. from six independent experiments. *C* and *D,* representative immunofluorescence images of mouse primary astrocytes under control conditions (*C*) and cultures subjected to 72 h treatment with 10 μM Aβ$_{25-35}$ (*D*) immunostained for Cx43 (*red*) and DAPI (*blue*). In control cultures, gap junctions typically appeared as puncta organized in *short lines* located at cell-cell junctions (*arrows*, *C*). In contrast, Aβ$_{25-35}$-treated astrocytes showed an obvious increase in intracellular Cx43 puncta scattered throughout the cytoplasm (*arrowheads*, *D*). *E,* scatter plot showing quantification of punctate areas in Aβ$_{25-35}$-treated astrocytes *versus* control cultures. Five to 10 fields were analyzed for each group from three independent cultures. *Error bars* denote mean ± S.D. with ***, $p = 0.0001$.

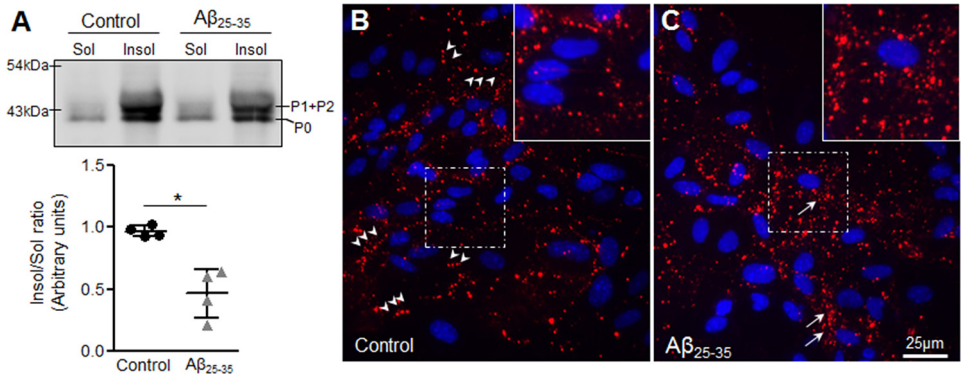

Figure 3. Effect of Aβ$_{25-35}$ on gap junction assembly of Cx43 in mouse astrocytes. *A,* representative immunoblot and scatter plot of membrane enriched fractions from control and Aβ$_{25-35}$ (10 μM, 72 h)-treated mouse primary astrocyte cultures subjected to Triton X-100 solubility assay and immunoblotted with anti-Cx43 antibody. Aβ$_{25-35}$-treated astrocytes show a significant reduction in Triton X-100–insoluble/soluble fraction ratio compared with control astrocytes suggesting a decrease in gap junction assembly. *Error bars* represent mean ± S.D. from four independent experiments with *, $p < 0.05$. *B* and *C,* representative immunofluorescence images of control (*B*) and Aβ$_{25-35}$ (10 μM, 72 h) treated (*C*) mouse primary astrocytes subjected to a *in situ* Triton X-100 solubility assay and immunolabelled for Cx43 (*red*) and DAPI (*blue*). Note that most of the punctate labeling at the cell–cell junctions representing the gap junctions are retained after Triton X-100 extraction in control astrocytes (*B*, *arrowheads and inset*). In the Aβ$_{25-35}$-treated astrocytes, the intracellular Cx43 pool shows insolubility following Triton X-100 extraction *in situ* (*C*, *arrows and inset*).

(Fig. 6, *E–I*). Thus, our results indicate that 4-PBA restores Cx43 expression at the cell surface typically in gap junctions with a parallel increase in functional gap junction coupling in Aβ-treated astrocytes.

Aβ does not affect cell surface trafficking of the newly synthesized Cx43 reaching the Golgi complex

Impaired gap junction communication could be either due to delay in trafficking of newly synthesized Cx43 to the plasma

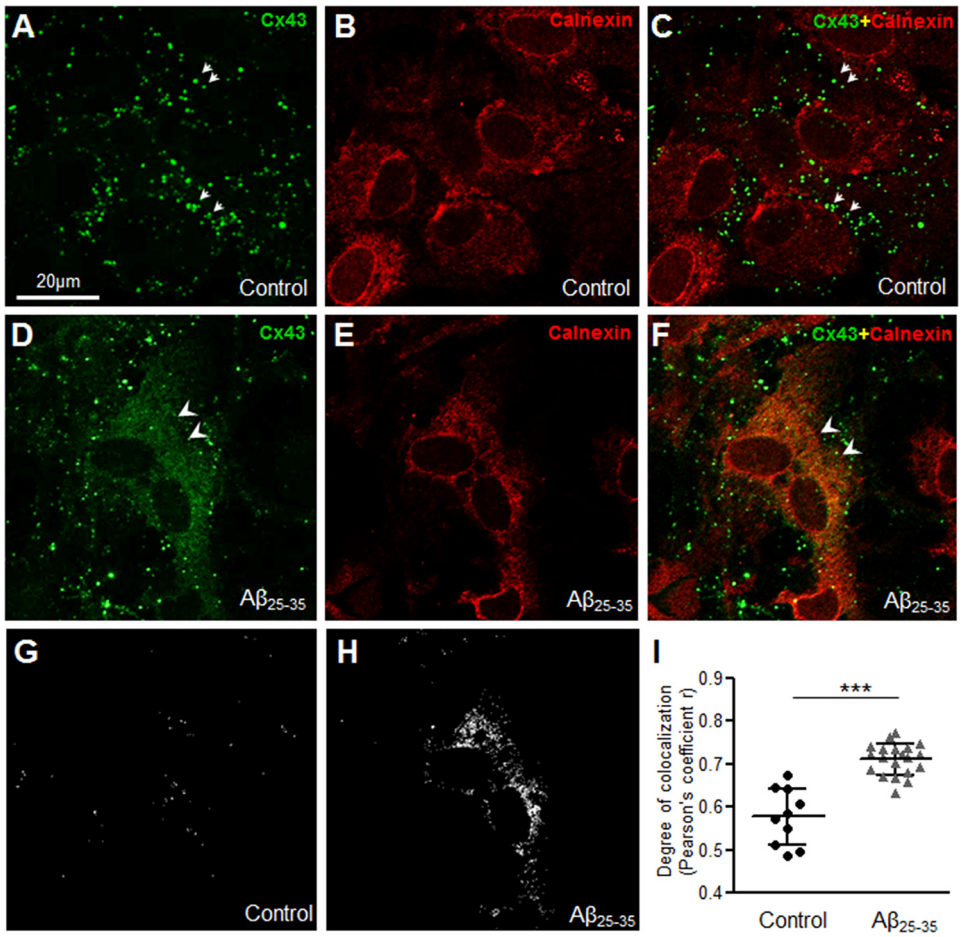

Figure 4. Aβ$_{25-35}$ increases Cx43 localization in the endoplasmic reticulum. *A–F*, representative confocal images of mouse primary astrocytes under control condition (*A–C*) or subjected to 72 h treatment with 10 μM Aβ$_{25-35}$ (*D–F*) double immunolabeled for anti-Cx43 (*green*) and ER marker anti-calnexin (*red*) antibodies. Control astrocytes show distinct punctate labeling not localized in the ER (*arrows*, *A* and *C*). Note the increased colocalization of Cx43 puncta with calnexin (*arrowheads*, *D* and *F*) in Aβ$_{25-35}$-treated astrocytes compared with control astrocytes. *G–I*, colocalization points between Cx43 and calnexin (*G* and *H*) and the degree of colocalization analysis (*I*) show a significant increase in Cx43 colocalization with calnexin in mouse astrocytes exposed to 10 μM Aβ$_{25-35}$ for 72 h compared with control. Five to 10 fields were analyzed for each group from two independent experiments. Data represent mean ± S.D. with ***, $p < 0.0001$.

membrane or increased internalization of the Cx43 gap junctions from the cell surface. To understand if the forward trafficking of the newly synthesized Cx43 channels from the Golgi to the plasma membrane could be affected by Aβ, we subjected control and Aβ$_{25-35}$-treated astrocytes to a brefaldin A (BFA) forward trafficking assay. Treatment with BFA induces a fast reversible inhibition of COPI-mediated transport from the ER to the Golgi (37). Control and Aβ-treated astrocytes were treated with 5 μg/ml of BFA for 8 h, and spatial distribution of Cx43 was analyzed by immunofluorescent labeling of Cx43 (Fig. 7, *A–F*). When control astrocytes were treated with BFA for 8 h, pre-existing gap junction plaques were not identifiable at the cell surface (Fig. 7*A*). Most of the Cx43 labeling was found accumulated in the perinuclear region both in control and Aβ$_{25-35}$-treated astrocyte cultures upon BFA treatment (Fig. 7, *A* and *D*). As expected, upon removal of BFA, transport of newly synthesized Cx43 was restored in control astrocyte cultures (Fig. 7, *B* and *C*). One hour after BFA removal, control astrocyte cultures still showed a lot of Cx43 labeling scattered throughout the cytoplasm and in the perinuclear region (Fig. 7*B*). Three hours post BFA removal, control astrocytes started showing Cx43 puncta organized into short lines typical of gap junctions indicating trafficking to the cell surface (Fig. 7*C*). Similarly, in Aβ$_{25-35}$-treated astrocyte cultures, 3 h after BFA removal Cx43 immunolabeling exhibited distinct punctate labeling away from the nucleus. These results indicated that further trafficking to the cell surface of the newly synthesized Cx43 that could reach the Golgi complex might not be affected by Aβ (Fig. 7*F*).

Aβ increases internalization of Cx43 gap junctions from the cell surface

The short $t_{1/2}$ of Cx43 makes functional gap junction communication between the coupled cells a highly dynamic process. The balance between the synthesis and degradation rate of Cx43 is an important way to control the level of functional gap junctions present at the cell surface. Cx43 internalization has been reported to be dependent on the dynamin GTPase activity (38, 39), which can be specifically blocked by the noncompetitive endocytosis inhibitor, Dynasore. First, to determine whether functional gap junction communication can be improved in Aβ-treated mouse astrocyte cultures by blocking endocytosis, we treated control and Aβ$_{25-35}$-treated cultures with Dynasore for 3 h (Fig. 8, *A–E*). Control cultures did not show any

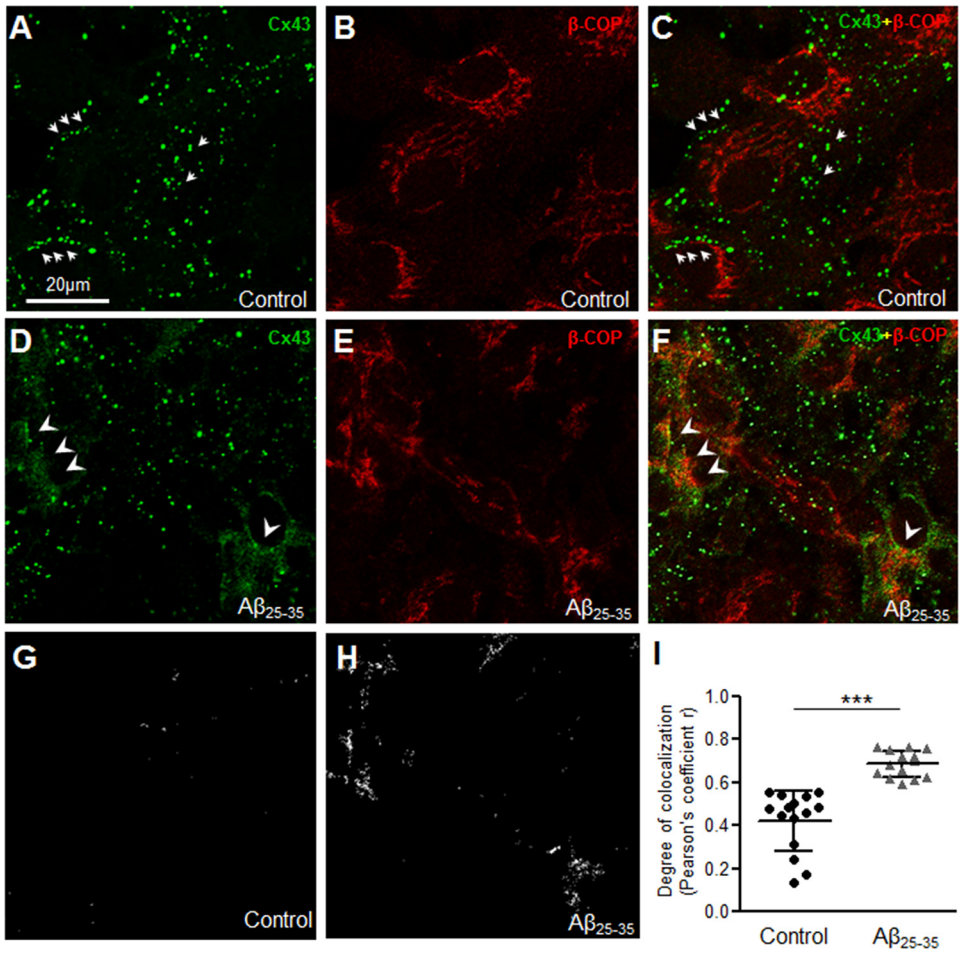

Figure 5. $A\beta_{25\text{-}35}$ increases Cx43 localization in the endoplasmic reticulum Golgi intermediate compartment. *A–F*, representative confocal microscope images of mouse primary astrocytes under control conditions (*A–C*) or subjected to 72 h treatment with 10 μM $A\beta_{25\text{-}35}$ (*D–F*) double immunolabeled for anti-Cx43 (*green*) and ERGIC marker anti-β-COP (*red*) antibodies. Control astrocytes show distinct punctate labeling not localized in the ERGIC (*arrows*, *A* and *C*). $A\beta_{25\text{-}35}$-treated astrocytes show increased co-localization of Cx43 puncta with β-COP (*arrowheads*, *D* and *F*) compared with control astrocytes. *G–I*, colocalization points between Cx43 and β-COP (*G* and *H*) and the degree of colocalization analysis (*I*) show a significant increase in Cx43 colocalization with β-COP in mouse astrocytes exposed to 10 μM $A\beta_{25\text{-}35}$ for 72 h compared with control. Five to 10 fields were analyzed for each group from two independent experiments. Data represent mean ± S.D. with ***, $p < 0.0001$.

significant alterations in Lucifer yellow dye transfer mediated through the gap junctions following Dynasore treatment. Interestingly, Dynasore intervention in $A\beta_{25\text{-}35}$-treated astrocytes demonstrated a marked improvement in Lucifer yellow dye transfer from the scrape loading line indicating that Aβ causes faster internalization of Cx43 from the cell surface (Fig. 8, *A–E*). Supporting this, our immunofluorescent labeling studies with anti-Cx43 antibody (Fig. 8, *F–I*) showed the presence of lined up Cx43 puncta typically representing the gap junctions in $A\beta_{25\text{-}35}$-treated astrocytes in the presence of Dynasore (Fig. 8*I*). $A\beta_{25\text{-}35}$-treated astrocytes in the absence of Dynasore exhibited Cx43 immunostaining scattered throughout the cell cytoplasm as shown earlier (Fig. 8*H*). Moreover, the cytoplasmic pool of Cx43 appeared to be less in $A\beta_{25\text{-}35}$-treated astrocytes exposed to Dynasore (Fig. 8*I*) compared with cultures without Dynasore (Fig. 8, *H* and *I*) confirming those to be internalized gap junctions.

To further determine whether the impaired gap junction communication in Aβ-treated astrocytes was because of the increased internalization rate of Cx43 rather than failed delivery to the plasma membrane, we first subjected the control and $A\beta_{25\text{-}35}$-treated astrocytes to BFA forward trafficking assay followed by Dynasore intervention during the 3-h BFA washout (Fig. 9). As expected, in the control astrocyte cultures functional gap junction communication was re-established upon restoring the secretory pathway with BFA washout for 3 h (Fig. 9, *A–E*). The presence of Dynasore in the culture medium during the 3-h BFA washout showed an additional increasing trend without reaching statistical significance in the dye travel distance compared with the BFA washout only cultures without Dynasore intervention. In contrast, the presence of Dynasore in the cell culture medium during the 3-h BFA washout in the $A\beta_{25\text{-}35}$-treated astrocytes significantly improved dye transfer mediated through the functional Cx43 gap junctions (Fig. 9, *F–J*). Taken together, these data suggest that Aβ increases endocytosis of Cx43 gap junctions thereby impairing functional gap junction communication between the mouse primary cultured astrocytes.

Aβ shows preferential binding affinity for Cx43

To further understand the mechanism by which Aβ modifies Cx43 gap junctions in astrocytes we used molecular docking

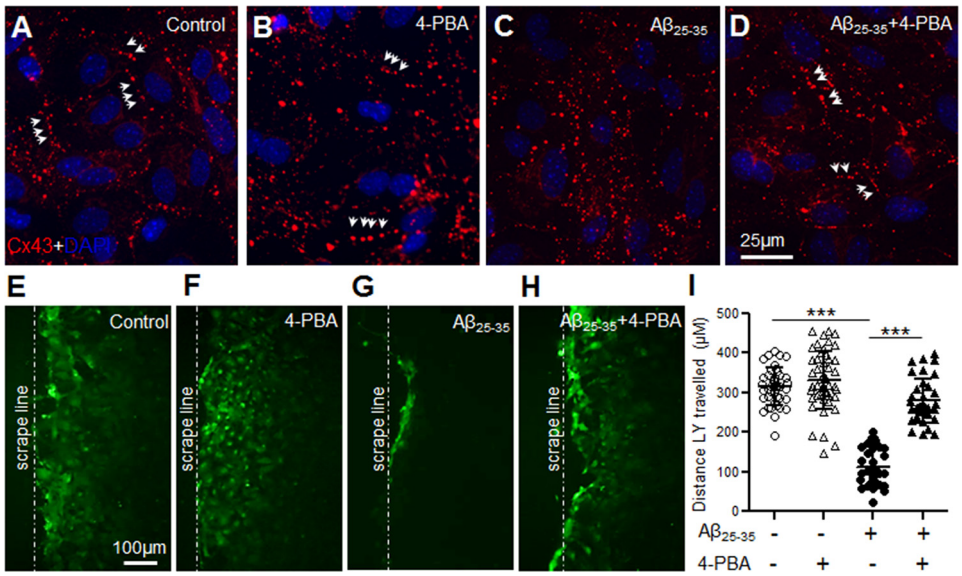

Figure 6. 4-Phenylbutyrate restores functional gap junction coupling in Aβ-treated astrocytes. *A–D,* representative immunofluorescence images depicting cellular distribution of Cx43 in mouse primary astrocytes under control conditions (*A*), 24 h treatment with 5 mM 4-PBA alone (*B*), 72 h treatment with 10 μM A$\beta_{25\text{-}35}$ alone (*C*), or 10 μM A$\beta_{25\text{-}35}$ (72 h) in combination with 4-PBA (5 mM, 24 h; *D*). Note the Cx43 labeling as *short lines* of puncta (*arrows*) typically representing gap junctions in A$\beta_{25\text{-}35}$-treated astrocyte cultures exposed to 4-PBA (*D*) similar to control (*A*) and 4-PBA treatment alone (*B*). Astrocytes exposed to A$\beta_{25\text{-}35}$ only, exhibit Cx43 labeling scattered throughout the cytoplasm (*C*). *E–H,* representative fluorescence micrographs of scrape loading and dye transfer assays with Lucifer yellow dye by astrocytes under control conditions (*E*), 24 h treatment with 5 mM 4-PBA alone (*F*), 72 h treatment with 10 μM A$\beta_{25\text{-}35}$ alone (*G*), or treatment with 10 μM A$\beta_{25\text{-}35}$ (72 h) in combination with 4-PBA (5 mM, 24 h; *H*). *I,* scatter plot depicting quantitation of scrape loading dye transfer assay showing a significant increase in dye transfer distance from the scrape loading line (*dashed line*) in A$\beta_{25\text{-}35}$-treated cultures subjected to 4-PBA compared with those exposed to A$\beta_{25\text{-}35}$ alone. 4-PBA alone did not show any significant difference compared with control cultures whereas astrocytes exposed to A$\beta_{25\text{-}35}$ only showed a significant reduction in dye transfer compared with control condition. *Error bars* denote mean ± S.D. of values from five to 10 fields each of four independent experiments with ***, $p < 0.0001$.

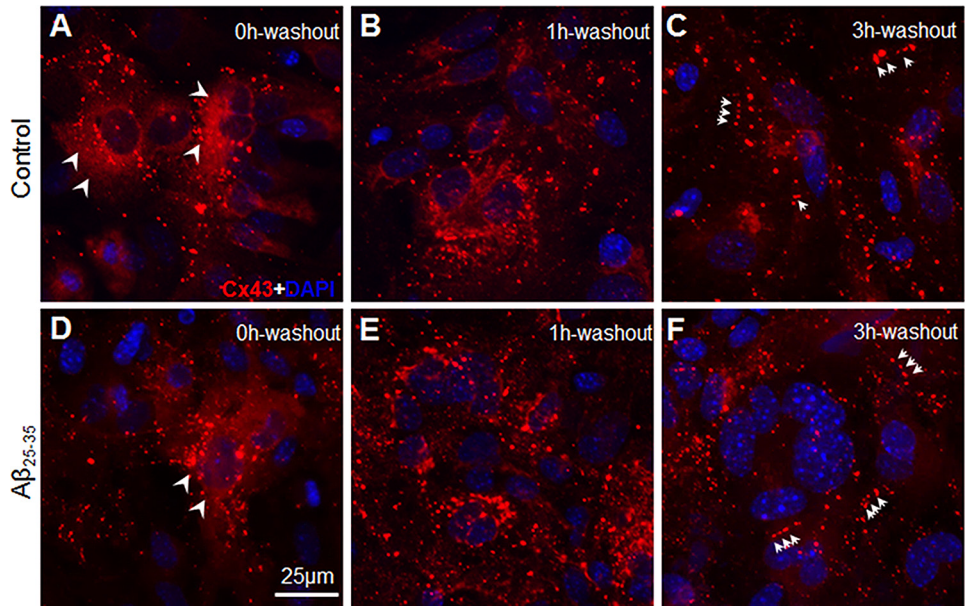

Figure 7. Effect of A$\beta_{25\text{-}35}$ on forward trafficking of Cx43 from Golgi to the cell surface. *A–F,* representative immunofluorescence images from three independent experiments of control (*A–C*) and A$\beta_{25\text{-}35}$-treated (*D–F*) mouse primary astrocytes exposed to 5 μg/ml of BFA for 8 h. Cells were fixed after BFA washout periods of 0, 1, or 3 h and immunostained for Cx43. Note that Cx43 immunostaining typically representing gap junction plaques were not identifiable in control astrocytes when treated with BFA for 8 h (*A*). Instead, Cx43 was found to be mostly distributed in a reticular like fashion in the perinuclear region (*arrowheads*, *A*) along with few puncta scattered in the cell cytoplasm. Three hours after BFA removal (*3h washout*, *C*) reticular staining pattern was much reduced and majority of Cx43 puncta were found to be organized into gap junctions at the cell–cell interface (*arrows*, *C*). Similarly, A$\beta_{25\text{-}35}$-treated astrocytes following 8 h of BFA exposure showed a diffused Cx43 immunostaining mostly in the perinuclear region (*arrowheads*, *D*). Note the Cx43 labeling in newly organized gap junctions in A$\beta_{25\text{-}35}$-treated astrocytes 3 h after BFA removal (*arrows*, *F*).

along with molecular dynamics simulation to reveal any possible interaction between Cx43 and full-length A$\beta_{1\text{-}42}$ or the A$\beta_{25\text{-}35}$ fragment (Fig. 10, *A–D*). Our results suggest that both A$\beta_{1\text{-}42}$ and A$\beta_{25\text{-}35}$ peptides have a high enthalpic preference for the Cx43 C-terminal tail region. The final conformations from both simulations (i.e Cx43 bound to either A$\beta_{1\text{-}42}$

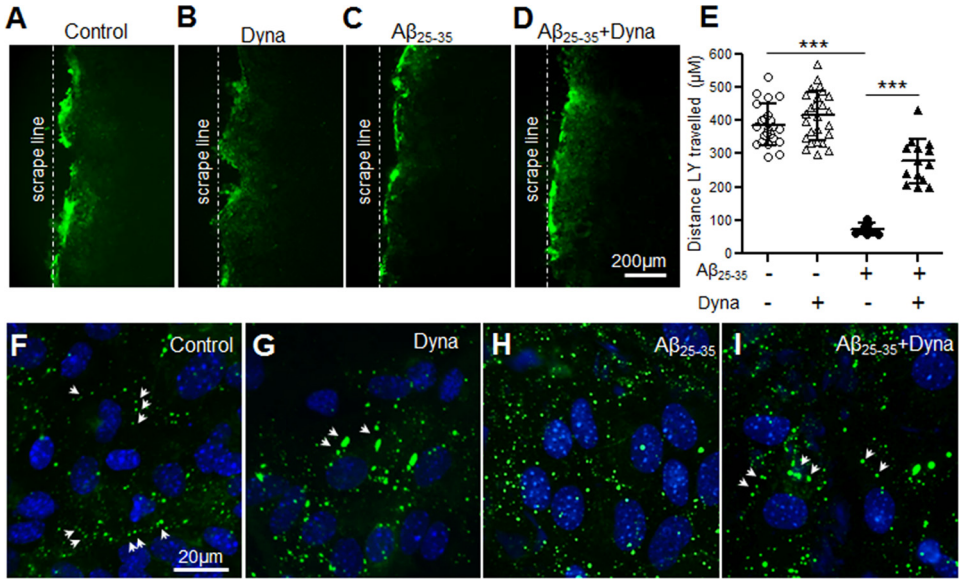

Figure 8. $A\beta_{25\text{-}35}$ increases endocytosis of Cx43 gap junctions impairing functional gap junction coupling. *A–D,* representative fluorescence micrographs of scrape loading and dye transfer assays with Lucifer yellow dye by astrocytes under control conditions (*A*), 3 h treatment with 80 μM Dynasore (*Dyna*) only (*B*), 72 h treatment with 10 μM $A\beta_{25\text{-}35}$ alone (*C*), or 72 h treatment with 10 μM $A\beta_{25\text{-}35}$ in combination with Dynasore (80 μM, 3 h; *D*). *E,* scatter plot depicting quantitation of scrape loading dye transfer assay showing a significant increase in dye transfer distance from the scrape loading line in $A\beta_{25\text{-}35}$-treated cultures subjected to Dynasore compared with those exposed to $A\beta_{25\text{-}35}$ alone. Dynasore alone did not show any significant difference compared with control cultures, whereas astrocytes exposed to $A\beta_{25\text{-}35}$ only showed a significant reduction in dye transfer compared with control condition. *Error bars* denote mean ± S.D. of values from four to eight fields each of three independent experiments with ***, $p < 0.0001$. *F–I*, representative immunofluorescence images depicting cellular distribution of Cx43 in mouse primary astrocytes under control conditions (*F*), 3 h treatment with 80 μM Dynasore (*Dyna*) only (*G*), 72 h treatment with 10 μM $A\beta_{25\text{-}35}$ alone (*H*), or 72 h treatment with 10 μM $A\beta_{25\text{-}35}$ in combination with Dynasore (80 μM, 3 h; *I*). Note the Cx43 labeling as short lines of puncta (*arrows*) typically representing gap junctions in $A\beta_{25\text{-}35}$-treated cultures exposed to Dynasore (*I*) similar to control (*F*) and only Dynasore-treated (*G*) astrocyte cultures. Astrocytes exposed to $A\beta_{25\text{-}35}$ only exhibit Cx43 labeling scattered throughout the cytoplasm (*H*).

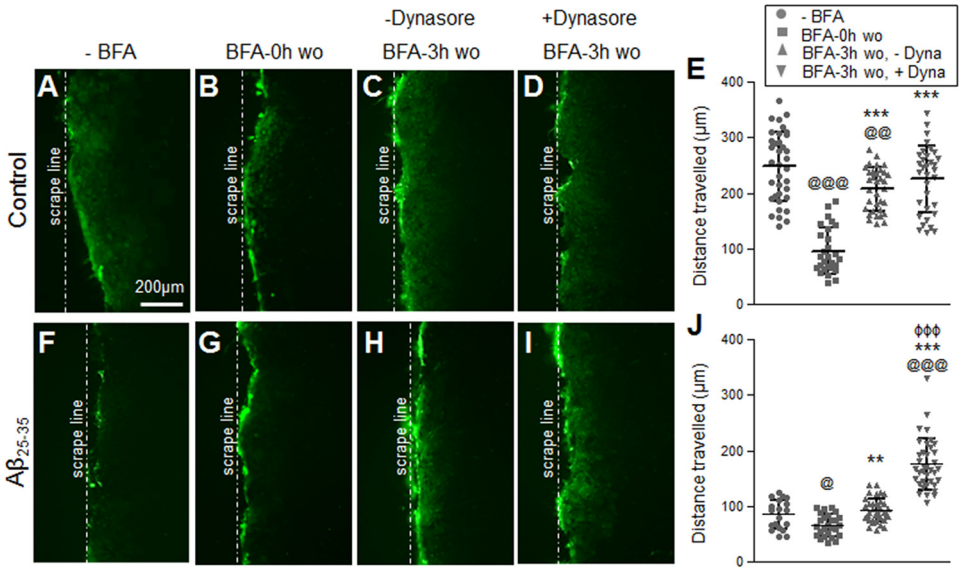

Figure 9. Inhibition of endocytosis during BFA forward trafficking assay recovers gap junction coupling in $A\beta_{25\text{-}35}$-treated astrocytes similar to control astrocytes. *A–J*, representative fluorescence micrographs and scatter plots of scrape loading and dye transfer assays with Lucifer yellow dye in control (*A–E*) and $A\beta_{25\text{-}35}$-treated (10 μM, 72 h) astrocytes (*F–J*) subjected to BFA forward trafficking assay in the presence or absence of 80 μM Dynasore (*Dyna*). Gap junction dye transfer is significantly reduced in control astrocytes with BFA (5 μg/ml, 8 h) compared with cultures without BFA treatment (*A versus B* and *E*). Note that functional gap junction communication is re-established in control astrocytes upon restoring the secretory pathway with a 3-h washout (*wo*) of BFA (*BFA 3h-wo*; *C* and *E*). The presence of Dynasore in the culture medium of control astrocytes during the BFA 3-h washout showed an increasing trend in the dye travel distance compared with the 3-h BFA washout in the absence of Dynasore (*C versus D* and *E*) and reached similar levels as in parallel cultures without BFA (*A*). $A\beta_{25\text{-}35}$-treated astrocytes without BFA (*F*) showed reduced gap junction dye transfer compared with control astrocytes under similar conditions (*A*). Exposure to BFA further reduced gap junction dye transfer in $A\beta_{25\text{-}35}$-treated astrocytes (*G* and *J*). BFA 3-h washout in $A\beta_{25\text{-}35}$-treated astrocytes (*H*) showed a significant increase in dye transfer compared with BFA treatment (*G* and *J*) but not with respect to $A\beta_{25\text{-}35}$ treatment alone (*F* and *J*). BFA 3-h washout in the presence of Dynasore significantly improved dye transfer in the Aβ-treated astrocytes (*I* and *J*). *Error bars* represent mean ± S.D. of values from six to 12 fields each from three independent experiments. @, $p < 0.05$; @@, $p < 0.01$; @@@, $p < 0.0001$ compared with respective cultures without BFA (−*BFA*); **, $p < 0.01$; ***, $p < 0.0001$ compared with cultures with BFA for 8 h (*BFA-0h wo*); $\phi\phi\phi$, $p < 0.0001$ compared with BFA 3h-wo without Dynasore (*BFA-3h wo*, *-Dyna*).

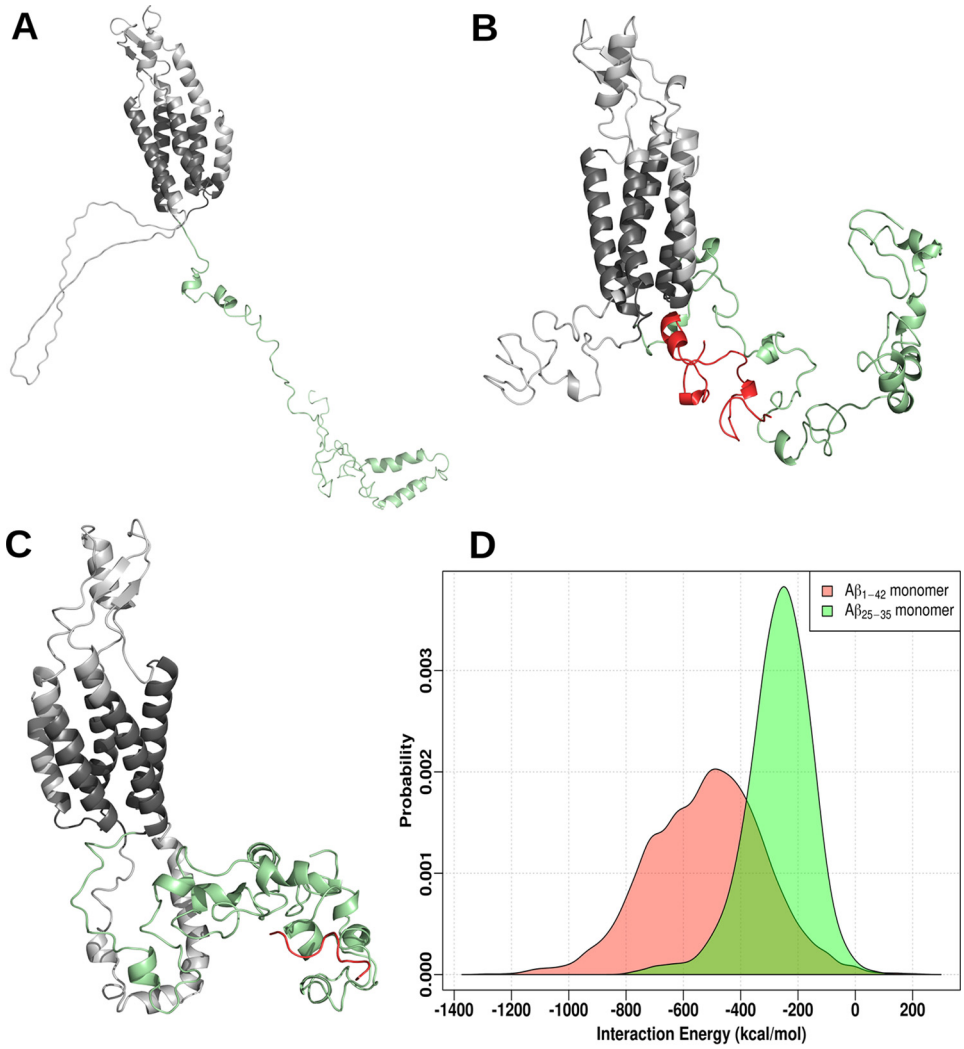

Figure 10. Molecular docking and simulations of monomeric Aβ with Cx43. *A,* homology modeled structure of mouse Cx43 with the lowest DOPE score. The protein is shown as a cartoon with the C terminus highlighted in *green*. *B* and *C,* the final conformations of Cx43 bound to $A\beta_{1\text{-}42}$ monomer (*red*, *B*), and $A\beta_{25\text{-}35}$ monomer (*red, C*). *D,* distribution of interaction energy between Cx43 and either $A\beta_{1\text{-}42}$ monomer or $A\beta_{25\text{-}35}$ monomer calculated from the last 50 ns data (energy in kcal/mol).

monomer or $A\beta_{25\text{-}35}$ monomer) are shown in Fig. 10, *B* and *C*. We also compared the interaction energy distributions of the last 50 ns of simulation data (Fig. 10*D*). Within the simulated time scales, both Aβ conformations bind favorably to Cx43, the binding free energies corresponding to $A\beta_{1\text{-}42}$ and $A\beta_{25\text{-}35}$ being −519.5 (±199.8) and −267.8 (±113.8) kcal/mol, respectively. Although these binding strengths indicate a very high affinity, a combination of enhanced sampling protocols and improved structural models may yield greater structural specificity along with further mechanistic details.

Discussion

In this study we investigated the underlying cellular mechanisms by which Aβ re-models the predominant astroglial gap junction protein Cx43 function in mouse primary cultured astrocytes. Our results indicate that exposure to 10 μM $A\beta_{25\text{-}35}$ for 72 h functionally uncoupled gap junction and hemichannel activity without altering Cx43 steady-state levels. Interestingly, $A\beta_{25\text{-}35}$ treatment caused an increase in intracellular Cx43 expression with a concomitant decrease in gap junction labeling. A major portion of this intracellular Cx43 expression was found to be resistant to Triton X-100 extraction indicating the presence of Cx43 aggregates and/or internalized gap junctions in line with reduced gap junctional coupling. Additionally, we found that a pool of the cytoplasmic Cx43 expression localized to the ER/ERGIC compartments. Supporting this treatment with 4-PBA, which is known to improve surface trafficking of several transmembrane proteins, restored Cx43 expression in gap junction plaques and functional gap junctional coupling in mouse primary astrocytes exposed to $A\beta_{25\text{-}35}$. Our data provide further evidence that the reduction in gap junction communication in $A\beta_{25\text{-}35}$-treated astrocytes was also caused by increased internalization of Cx43 from the cell surface via endocytosis and not due to the impaired delivery of Cx43 from the Golgi to the cell surface. Furthermore, using molecular dynamic simulations we showed that Aβ might bind Cx43, thus mediating the observed effects. Thus, this study provides new insights into the cellular mechanisms underlying altered Cx43 function in astrocytes exposed to Aβ peptides.

Aβ-mediated altered Cx43 trafficking in astrocytes

Earlier studies have suggested that both reactive astrogliosis and increase in Aβ levels, the two key neuropathological features that characterize all AD brains, are associated with altered astrocytic connexin channel functions subsequently leading to neuronal damage (21–24, 27). Accumulating evidence indicates that gap junctions and hemichannels are oppositely regulated in several neuropathological conditions (40). In line with this inverse correlation, we observed that $A\beta_{25\text{-}35}$ significantly reduced astrocyte–astrocyte gap junction communication as examined by intercellular Lucifer yellow dye transfer and increased hemichannel activity measured by ethidium bromide dye uptake. Cx43 mRNA and total protein levels including the pattern of immunoreactive bands did not show any significant difference between $A\beta_{25\text{-}35}$-treated and control astrocyte cultures. Thus, the modulations in dye transfer and dye uptake induced by $A\beta_{25\text{-}35}$ were not due to changes in Cx43 levels or its altered phosphorylation state detectable by shifts in Cx43 electrophoretic mobility. Interestingly, our immunolabeling studies showed a clear distinction in the Cx43 cellular distribution in $A\beta_{25\text{-}35}$-treated mouse astrocytes compared with control cultures. Although we showed that the expression pattern of Cx43 puncta characteristic of gap junction plaques appeared to be reduced in $A\beta_{25\text{-}35}$-treated astrocytes, a simultaneous increase in the intracellular Cx43 labeling explained the reduced astroglial gap junction coupling. Moreover, many of these Cx43 puncta were found to be resistant to Triton X-100 extraction at 4 °C, suggesting intracellular Cx43 aggregates and/or internalized gap junctions that do not contribute to functional gap junction coupling.

The life cycle of Cx43 involves post-translational insertion of Cx43 monomers into the ER membrane followed by their oligomerization into hexameric hemichannels or connexons in the Golgi. Preassembled hemichannels are translocated to the cell surface, which then dock with connexons from an apposing cell and undergo channel clustering to form morphologically identifiable gap junction plaques (41). Cx43 is unique in that it does not oligomerize in the ER unlike most multimeric membrane proteins. Instead, it exists as monomers in the ER membrane where Cx43 is stabilized by at least one or more protein chaperones that prevent its premature oligomerization in the ER (36, 42). Premature oligomerization in the ER can cause Cx43 aggregation leading toward its degradation by the proteasomal pathway thereby causing reduced gap junction coupling. Our immunolabeling studies showed an increased co-localization of Cx43 with the ER marker calnexin and ERGIC marker β-COP in $A\beta_{25\text{-}35}$-treated astrocytes compared with control astrocytes pointing toward a reduced ER function in proper trafficking of Cx43 along the secretory pathway. Supporting this, our results indicate that treatment with 4-PBA can play an important role in improving gap junction coupling in $A\beta_{25\text{-}35}$-treated astrocytes. 4-PBA, a well-established histone deacetylase inhibitor, improves the trafficking of several transmembrane proteins, including Cx43, an effect that is mediated through the modulation of ER-associated chaperones like ERp29 (34–36). Thus, it is possible that 4-PBA alters expression of one or more proteins of the Cx43 quality control pathway that regulates proper folding and trafficking of Cx43 to the cell surface, thereby restoring the impaired gap junction communication between astrocytes following $A\beta_{25\text{-}35}$ treatment. Interestingly, several recent studies have reported that administration of 4-PBA in established mouse models of AD exerted neuroprotective effects and reversed AD-associated phenotypes including cognitive deficits (43–45). Thus, 4-PBA, a drug already approved for clinical use in treating urea cycle disorders (46) has been proposed to provide a novel approach for the treatment of AD. However, the underlying molecular mechanisms by which 4-PBA offers neuroprotection in AD is not fully understood and needs further investigation.

Depending on the cell type studied, Cx43 has a very short $t_{1/2}$ ranging from 1.5 to 5 h (47–49). This makes gap junctions highly dynamic plasma membrane domains with fast turnover rates. Thus the amount of gap junctions and hemichannels present on the cell surface is largely determined by a balance between the formation and removal of such channels from the plasma membrane. Removal of gap junctions from the plasma membrane involves internalization of the entire junctional complex in the form of double membrane annular junctions that are targeted to lysosomes for degradation (50–53). Among the many processes involved in the removal of gap junctions, the clathrin machinery has been reported to play a major role in gap junction internalization. Notably, clathrin has been detected on Cx43 GJs by immunofluorescence and silencing of clathrin and the adaptor proteins, AP-2 and Dab2, or the GTPase dynamin caused cells to harbor fewer annular gap junctions (38, 39). Interestingly, our results using a dynamin blocker, Dynasore, clearly showed that gap junction communication between the astrocytes measured by Lucifer yellow dye transfer was significantly restored in cultures exposed to $A\beta_{25\text{-}35}$. Supporting this, Cx43 immunolabeling showed elevated gap junction labeling in $A\beta_{25\text{-}35}$-treated astrocytes in the presence of Dynasore compared with those without Dynasore intervention. This is further in line with our observations from *in situ* Triton X-100 solubility assays, showing Triton X-100 resistant Cx43 cytoplasmic labeling in $A\beta_{25\text{-}35}$-treated astrocytes, indicating that these could be internalized Cx43 gap junctions. In addition, we have used BFA to separate the processes of formation and removal of gap junctions from the cell surface. Our results using dye transfer and immunolabeling studies showed that delivery of newly synthesized Cx43 from the Golgi to the cell surface was not affected in the presence of $A\beta_{25\text{-}35}$. Thus, our findings clearly indicate that $A\beta_{25\text{-}35}$ increases endocytosis of Cx43 gap junctions from the cell surface, thereby reducing functional gap junction coupling between the astrocytes. Additionally, our molecular dynamics simulation studies suggest that both $A\beta_{1\text{-}42}$ and $A\beta_{25\text{-}35}$ monomers have a high enthalpic preference for the C-terminal tail region of Cx43. This is particularly interesting given that the C-terminal tail of Cx43 is known to interact with several other proteins that modulate its intracellular trafficking and channel gating (54). However, the mechanistic details of Aβ-Cx43 binding and the role of such interactions in the intracellular trafficking and function of Cx43 need to be established in future studies.

In summary, we have demonstrated that Aβ causes intracellular retention of Cx43 as well as rapid internalization of Cx43 gap junctions from the cell surface in mouse primary cultured astrocytes. Both of these phenomena can negatively affect Cx43

Table 1
List of antibodies used in the study

Antibody	Application[a]	Dilution	Source
Connexin 43 (polyclonal)	WB	1:8000	Sigma-Aldrich
	IF	1:800	
Connexin 43 (monoclonal)	IF	1:400	Sigma-Aldrich
GFAP (polyclonal)	IF	1:200	Sigma-Aldrich
	FC	1:50	
β-Actin (monoclonal)	WB	1:5000	Sigma-Aldrich
Calnexin (polyclonal)	IF	1:400	Abcam
β-COP (polyclonal)	IF	1:400	ThermoFisher Scientific
Goat anti-rabbit horseradish peroxidase	WB	1:5000	Jackson ImmunoResearch Laboratory
Goat anti-mouse horseradish peroxidase	WB	1:5000	Jackson ImmunoResearch Laboratory
Goat anti-rabbit Alexa Fluor 568	IF	1:1000	ThermoFisher Scientific
Goat anti-mouse Alexa Fluor 488	IF	1:1000	ThermoFisher Scientific

[a] The abbreviations used were: WB, Western blotting; IF, immunofluorescence; FC, flow cytometry.

channel function at the cell surface subsequently leading to astrocytic and neuronal damage. Although impaired gap junction coupling can restrict the propagation gap junction permeable prosurvival molecules such as those involved in energy homeostasis (glucose and ATP), and free radical scavengers (ascorbic acid and reduced GSH), an emerging theory in the field suggests that increased Cx43 hemichannel activity in astrocytes causes excessive release of ATP and glutamate that can directly cause neuronal death. Thus, several recent studies have indicated Cx43 gap junctions/hemichannels as a potential therapeutic target in reducing neuronal damage without much attention to the underlying mechanisms by which Cx43 can be modified during the disease. This is particularly important given that the Cx43 forms both gap junction channels and hemichannels, and the functional consequences of Cx43 modifications are manifold. The current study provides novel insights into the cellular mechanisms by which Aβ affects Cx43 function in astrocytes, which can be crucial for the development of therapeutic strategies aimed at restoring neuronal homeostasis.

Experimental procedures

Reagents

The bicinchoninic acid (BCA) protein assay kit, enhanced chemiluminescence kit, ProLong Gold anti-fade reagent, Lucifer yellow, DNase I, High Capacity cDNA Reverse Transcription kit, and DyNAmo Color Flash SYBR Green qPCR kit were purchased from ThermoFisher Scientific. Mouse *Cx43* and *β-actin* primers for quantitative PCR were from Integrated DNA Technologies, Inc. $A\beta_{25\text{-}35}$ and $A\beta_{35\text{-}25}$ peptides were from Bachem AG. RNA isolation kit was purchased from Qiagen. Poly-L-lysine, DNase I (cell culture grade), BFA, Dynasore, 4-PBA, and protease and phosphatase inhibitor cocktails were obtained from Sigma-Aldrich. All cell culture reagents including Dulbecco's modified Eagle's medium, Hank's balance salt solution (HBSS), fetal bovine serum (FBS), 0.25% trypsin and penicillin/streptomycin were procured from Gibco, ThermoFisher Scientific. BD CytoFix Fixation buffer and BD Perm/Wash Buffer were obtained from BD Biosciences. Sources of all the primary and secondary antibodies used in the study are listed in Table 1. All other chemicals were from Sigma-Aldrich or ThermoFisher Scientific.

Primary astrocyte culture

Primary astrocyte cultures were prepared from postnatal day 0-1 mouse pup brains as previously described with minor modifications (55). Briefly, following removal of the olfactory bulbs, cerebellum, and meninges, brain tissue was dissociated in Ca^{2+} and Mg^{2+}-free HBSS with 0.25% trypsin and 50 μg/ml of DNase I at 37 °C for 30 min with shaking. Trypsin was neutralized by adding 0.25% FBS and followed by a wash at 300 × *g* for 10 min. The pellet was resuspended in HBSS and the cell suspension was passed through a 70-μm cell strainer. Cells were seeded onto T25 flasks in astrocyte growth medium containing Dulbecco's modified Eagle's medium supplemented with 10% FBS and 1% penicillin/streptomycin. Medium was replaced 24 h after plating to remove all nonadherent cells and every third day thereafter. Primary astrocytes reached about 90% confluence at 8-9 days *in vitro* following which addition of fresh media was stopped for the next 10 days to allow differential adhesion of astrocytes and microglia. Subsequently, culture flasks were shaken vigorously in an orbital incubator shaker at 200 rpm for 45 min at 37 °C to dislodge the loosely adherent microglia growing on top of the strongly adherent astrocyte monolayer. The media was discarded and astrocytes were collected following trypsinization and plated for experiments. The enriched cultures from three independent culture batches were quantified for GFAP-positive astrocytes by flow cytometry (described later), which showed that cultures contained 97.45 ± 0.41% (mean ± S.D.) of GFAP-positive astrocytes (Fig. S2). Cultures established from different breeding pairs were used for each set of experiments. All experiments were approved by the Institutional Animal Care and Use Committee and conducted in accordance with the guidelines constituted by the Committee for the Purpose of Control and Supervision of Experiments on Animals (CPCSEA, Goverment of India).

Cell culture treatments

Primary astrocyte cultures at 80–90% confluence were treated with 10 μM $A\beta_{25\text{-}35}$ or $A\beta_{35\text{-}25}$ reverse peptides dissolved in cell culture grade water and kept in normal culture conditions for 24-72 h following previously published protocols (24). Control and $A\beta_{25\text{-}35}$-treated mouse primary astrocyte cultures were incubated with 4-PBA (5 mM, 24 h), BFA (5 μg/ml, 8 h), or Dynasore (80 μM, 3 h) where indicated. For BFA forward trafficking assays, control and $A\beta_{25\text{-}35}$-treated mouse primary

astrocytes were treated with 5 μg/ml of BFA for 8 h, washed, and then allowed to recover for the indicated durations (1-3 h) in the presence or absence of Dynasore (80 μM).

Flow cytometry

Confluent astrocyte cultures were trypsinized and washed twice in flow buffer (PBS containing Ca^{2+}/Mg^{2+} and 2% FBS). Following centrifugation at 300 × *g* for 5 min at 4 °C, cells were resuspended in flow buffer and approximately 1 × 10^6 cells were added to each 5-ml polystyrene round bottom FACs tubes. Cells were fixed in 100 μl of BD CytoFix Fixation buffer for 15 min at room temperature. Following a wash with flow buffer, cells were incubated with rabbit anti-GFAP antibody (1:50) diluted in BD Perm/Wash Buffer for 30 min at room temperature. Subsequently, cells were washed three times in BD Perm/Wash Buffer and labeled with goat anti-rabbit FITC-conjugated secondary antibody (1:50) for 30 min at room temperature. After a final wash, cells were resuspended in 500 μl of flow buffer and subjected to flow cytometry using a BD FACSVerse™ flow cytometer. Ten thousand to 50,000 events were collected for each tube assayed and the data were analyzed using BD FACSuite analysis software (55). The experiments were performed from three independent cultures.

RNA isolation and real-time PCR

RNA was isolated using RNeasy RNA extraction kit following the manufacturer's instructions (Qiagen). RNA (0.5-1 μg) was treated with DNase I and reverse transcribed using High Capacity cDNA Reverse Transcription kit following manufacturer's protocol. Quantitative real-time PCR was performed with DyNAmo Color Flash SYBR Green master mix using QuantStudio 3 Real-Time PCR System (Applied Biosystems, ThermoFisher Scientific) with the following cycling conditions: initial denaturation at 95 °C for 7 min followed by 40 cycles at 95 °C for 10 s and 60 °C for 30 s. Primer sequences used were: *Connexin 43* (forward, 5′-CCCTTCACGCGATCCTTA-3′ and reverse, 5′-TCATGCTGGTGGTGTCCTTG-3′) and *β-actin* (forward, 5′-GTGACGTTGACATCCGTAAAGA-3′ and reverse, 5′-GCCGGACTCATCGTACTCC-3′). Experiments were performed from four independent cultures and each sample was assayed in duplicate and mRNA normalized to *β-actin* mRNA. Relative gene expressions were calculated using the comparative C_T method ($2^{-\wedge\wedge C_T}$) (56).

Western blotting

Confluent monolayers of astrocytes were homogenized in ice-cold radioimmunoprecipitation (RIPA) lysis buffer (50 mM Tris base, 150 mM NaCl, 0.1% SDS, 1% Triton X-100, 0.5% sodium deoxycholate, pH 7.4) containing protease and phosphatase inhibitor cocktails. Protein concentrations were determined using BCA protein assay kit following the manufacturer's instructions. Protein samples (5 μg) were resolved on 12% SDS-polyacrylamide gel and transferred to polyvinylidene difluoride membranes. Membranes were blocked with 10% skimmed milk for 1 h at room temperature and incubated overnight at 4 °C with anti-Cx43 antibody. Following three washes in Tris-buffered saline containing 0.1% Tween-20 (TBST), membranes were incubated with horseradish peroxidase-conjugated secondary antibodies and immunoreactive proteins were visualized using SuperSignal™ West Pico PLUS enhanced chemiluminescence kit. All blots were re-probed with anti-β-actin antibody to monitor equal protein loading and densitometry was performed using NIH ImageJ gel analysis tool (57). Experiments were performed from six independent cultures and each sample was loaded in duplicate.

Immunofluorescence and confocal microscopy

Cells grown on glass coverslips were fixed with 4% paraformaldehyde for 15 min at room temperature and washed three times with PBS. Fixed cells were permeabilized with 0.25% Triton X-100 in PBS for 15 min at room temperature and blocked with PBS containing 0.1% Triton X-100 and 1% BSA for 1 h at room temperature. Cells were incubated overnight at 4 °C with anti-Cx43 antibody combined with anti-GFAP, anti-calnexin, or anti-β-COP antibodies (at dilutions listed in Table 1) diluted in PBS with 0.1% Triton X-100 and 0.25% BSA and subsequently labeled with Alexa Fluor 488- and/or 568-conjugated secondary antibodies for 2 h at room temperature. Coverslips were washed three times with PBS and mounted in ProLong Gold anti-fade reagent. Immunostained cells were visualized and imaged using an Olympus IX-81 inverted epifluorescence microscope. For colocalization studies, imaging of double-immunolabeled cells were performed using a Leica SP8 confocal laser scanning microscope (Leica Microsystems GmbH, Wetzlar, Germany) equipped with a HC PL APO ×63 oil-immersion objective lens using 488- and 552- nm laser lines. Images were acquired and processed using LasX software (Leica Microsystems). Image analysis was done using ImageJ software (57). The determination of colocalization of Cx43 and the ER marker, calnexin, or the ERGIC marker, β-COP, was carried out by using ImageJ Colocalization Threshold plug-in. Pearson's coefficient for colocalization was calculated that compares a pair of images from different fluorescent channels. Five to 10 fields were analyzed for each group from two independent experiments.

Triton X-100 solubilization assay

Cx43 assembly into gap junctions was analyzed using Triton X-100 detergent solubility assay (33). Primary astrocytes were harvested in ice-cold PBS containing protease and phosphatase inhibitor cocktails. Cells were homogenized using a ball bearing cell homogenizer. Protein concentrations were determined using BCA protein assay kit and equal amounts of protein for $A\beta_{25\text{-}35}$-treated and control groups were centrifuged at 100,000 × *g* for 1 h at 4 °C using a Beckman Optima Max ultracentrifuge (Beckman Coulter Inc., Brea, CA) to obtain a membrane-enriched pellet. For detergent solubilization, the membrane-enriched pellet was resuspended in PBS containing 1% Triton X-100 and incubated at 4 °C for 30 min. The samples were centrifuged at 100,000 × *g* for 30 min at 4 °C and separated into Triton X-100–soluble supernatant and Triton X-100–insoluble pellet. The pellet was resuspended in lysis buffer containing 1% SDS and solubilized by sonication (Triton X-

Table 2
Sequence homology of Cx43 with other connexins

Mouse connexin 43[a]	Other connexins (PDB ID)[a]	% Identity
$Cx43_{1\text{-}231}$	Lamb connexin $46_{2\text{-}222}$ (6MHQ)	51.5
$Cx43_{234\text{-}258}$	Human connexin $43_{1\text{-}26}$ (2LL2)	80.8
$Cx43_{251\text{-}382}$	Rat connexin $43_{1\text{-}132}$ (1R5S)	98.5

[a]The amino sequence region is shown as a subscript.

100–insoluble fraction). Equal volumes of soluble and insoluble fractions were resolved on 12% SDS-PAGE gel and analyzed for Cx43 levels by immunoblotting. Experiments were performed from four independent cultures.

For detergent extraction *in situ*, confluent astrocyte monolayers grown on poly-L-lysine–coated coverslips were rinsed with PBS and incubated in ice-cold PBS containing 1% Triton X-100 for 30 min at 4 °C with gentle shaking. The control cells were treated similarly without 1% Triton X-100. The coverslips were fixed with 4% paraformaldehyde for 15 min at room temperature and immunolabeled with anti-Cx43 antibody as described earlier. Experiments were performed from three independent cultures.

Dye transfer assay

Gap junction mediated intercellular coupling was evaluated by transfer of Lucifer yellow dye in a scrape loading assay as described previously (55). Briefly, completely confluent monolayer cultures of control and $A\beta_{25\text{-}35}$-treated astrocytes grown on 35-mm culture dishes were scrape loaded with Lucifer yellow dye and incubated at room temperature for 1 min. The cells were then rinsed quickly three times with PBS and incubated at 37 °C for an additional 8 min in the growth media to allow the loaded dye to transfer to adjoining cells. Fluorescent images were captured using an Olympus® IX-81 epifluorescence microscope with a UV filter. The distance traveled by the dye in different treatments was measured from the scrape line using ImageJ software (57). Five to 10 fields were analyzed for each group from three to four independent experiments.

Dye uptake assay

Dye uptake assay using ethidium bromide (EtBr) was done to study the hemichannel activity (24). The cells grown to ~70% confluence were washed with Locke's solution (154 mM NaCl, 5.4 mM KCl, 2.3 mM $CaCl_2$, 5 mM HEPES buffer, pH 7.4) after removing media and were treated with Locke's solution containing 5 μM EtBr for 10 min at 37 °C. Subsequently, the cells were fixed in 4% paraformaldehyde and proceeded with normal immunofluorescence protocol as described above to probe with anti-GFAP antibody. The cells were mounted with mounting medium without DAPI (Vectashield, Vector Laboratories Inc., Burlingam, CA). Cells were imaged using Olympus® IX-81 epifluorescence microscope and the intensity of the nuclei was quantified using ImageJ software (57). Five to 10 fields were analyzed for each group from three independent experiments.

Homology modeling

The primary sequence of mouse Cx43 was obtained from the Uniprot Knowledgebase (accession number P23242). Cx43 is 382 amino acids long and shares homology with various connexins (Table 2). Because no single template structure shares very high sequence homology with the whole Cx43, multiple templates (Table 2) were used along with the MODELLER package (58) for the Cx43 model building. We have generated 20 models and the model with the lowest DOPE score (59) was further used for docking studies.

Docking and molecular dynamics simulations

Being an intrinsically disordered peptide, the conformation of Aβ is subject to its surrounding environment and peptide length (60). A previously reported monomeric structure of $A\beta_{1\text{-}42}$ (61–63) was used in docking studies with Cx43. The $A\beta_{25\text{-}35}$ segment was extracted from the full-length monomer Aβ, as the conformation of this segment in fully aqueous environment remains experimentally unreported. Both structures were consequently used for blind docking with Cx43 using the ZDOCK server (64). The transmembrane helices of Cx43 were excluded for docking interaction.

The best ranked docked poses of Cx43 with either $A\beta_{1\text{-}42}$ monomer or $A\beta_{25\text{-}35}$ monomer were further used as the initial structure for performing implicit solvent molecular dynamics simulations. All simulations were carried out in the AMBER16 (65) program suite. The Cx43 and Aβ were prepared with AMBER ff14SB force field (66) and the effect of water was implemented using the generalized Born model (67). A 1000 steps of steepest descent energy minimization was followed by another 1000 steps of conjugate-gradient minimization without any constraint. We have performed 200 ps of equilibration where the system temperature was raised from 0 to 310 K using a Langevin thermostat. This was followed by a 100-ns production run in NVT condition where coordinates were saved every 5 ps. Throughout the equilibration and production run the four transmembrane helices of the Cx43 were constrained by applying a harmonic force of 1 kcal/mol to main chain atoms. During the simulation, the infinite cutoff was used to calculate the nonbonded interaction energy, and SHAKE (68) was used to restrain the bonds involving hydrogen atoms. Interaction energy of the last 50 ns of data, were calculated using the NAMD Energy plugin (69).

Statistical analysis

All data are presented as mean ± S.D. and data are represented as points in the scatter plot. Statistical significance was determined by one-way analysis of variance followed by Newman-Keuls post hoc analysis for multiple comparisons or unpaired two-tailed Student's *t* test for single comparison with a significance threshold of $p < 0.05$. All analyses were performed using GraphPad Prism version 5.0 software (GraphPad Software, Inc., La Jolla, CA).

Data availability

The data that support the findings of this study are all contained in the results section of the manuscript.

Acknowledgments—We thank the Wellcome Imaging confocal microscopy facility supported by DBT-Wellcome Trust India Alliance

grant number IA/I/16/1/502369 (to Dr. Arnab Gupta) and also the IISER-K cell imaging and animal facilities.

Author contributions—M. M. and J. D. S. conceptualization; M. M. and J. D. S. resources; M. M., L. V., A. B., S. D. C., and N. S. formal analysis; M. M., N. S., and J. D. S. supervision; M. M. and J. D. S. funding acquisition; M. M., L. V., A. B., and S. D. C. investigation; M. M., L. V., A. B., S. D. C., N. S., and J. D. S. visualization; M. M., L. V., A. B., S. D. C., and N. S. methodology; M. M., L. V., and S. D. C. writing-original draft; M. M. project administration; M. M., N. S., and J. D. S. writing-review and editing; N. S. software.

Funding and additional information—This work was supported by Science and Engineering Research Board, India Grant YSS/2015/000486 (to M. M.) and research funds (to J. D. S.) from the Indian Institute of Science Education and Research Kolkata (IISER-K), India. M. M. is a recipient of DBT-Wellcome Trust India Alliance Early Career Fellowship. L. V. is a recipient of an Institutional fellowship from IISER-K. A. B. is a recipient of Senior Research Fellowship from Council for Scientific and Industrial research (CSIR), India. S. D. C. is a recipient of CSIR Research Associate fellowship. N. S. acknowledges computational resources procured with funds from SERB Grant EMR/2016/001108.

Conflict of interest—The authors declare that they have no conflicts of interest with the contents of this article.

Abbreviations—The abbreviations used are: Cx43, connexin 43; AD, Alzheimer disease; Aβ, amyloid-β; ER, endoplasmic reticulum; GFAP, glial fibrillary acidic protein; 4-PBA, 4-phenylbutyrate; BFA, brefaldin A; BCA, bicinchoninic acid; HBSS, Hank's balance salt solution; ERGIC, ER Golgi intermediate compartment; DAPI, 4′,6-diamidino-2-phenylindole.

References

1. Barres, B. A. (2008) The mystery and magic of glia: a perspective on their roles in health and disease. *Neuron* **60,** 430–440 CrossRef Medline
2. Nagy, J. I., and Rash, J. E. (2000) Connexins and gap junctions of astrocytes and oligodendrocytes in the CNS. *Brain Res. Rev.* **32,** 29–44 CrossRef Medline
3. Pannasch, U., Vargová, L., Reingruber, J., Ezan, P., Holcman, D., Giaume, C., Sykova, E., and Rouach, N. (2011) Astroglial networks scale synaptic activity and plasticity. *Proc. Natl. Acad. Sci. U.S.A.* **108,** 8467–8472 CrossRef Medline
4. Rouach, N., Koulakoff, A., Abudara, V., Willecke, K., and Giaume, C. (2008) Astroglial metabolic networks sustain hippocampal synaptic transmission. *Science* **322,** 1551–1555 CrossRef Medline
5. Scemes, E., and Giaume, C. (2006) Astrocyte calcium waves: what they are and what they do. *Glia* **54,** 716–725 CrossRef Medline
6. Wallraff, A., Köhling, R., Heinemann, U., Theis, M., Willecke, K., and Steinhäuser, C. (2006) The impact of astrocytic gap junctional coupling on potassium buffering in the hippocampus. *J. Neurosci.* **26,** 5438–5447 CrossRef Medline
7. Alexander, D. B., and Goldberg, G. S. (2003) Transfer of biologically important molecules between cells through gap junction channels. *Curr. Med. Chem.* **10,** 2045–2058 CrossRef Medline
8. Goodenough, D. A., and Paul, D. L. (2009) Gap junctions. *Cold Spring Harb. Perspect. Biol.* **1,** a002576 CrossRef Medline
9. Cheung, G., Chever, O., and Rouach, N. (2014) Connexons and pannexons: newcomers in neurophysiology. *Front. Cell Neurosci.* **8,** 348 CrossRef Medline
10. Spray, D. C., Ye, Z. C., and Ransom, B. R. (2006) Functional connexin "hemichannels": a critical appraisal. *Glia* **54,** 758–773 CrossRef Medline
11. Bosch, M., and Kielian, T. (2014) Hemichannels in neurodegenerative diseases: is there a link to pathology? *Front. Cell. Neurosci.* **8,** 242 CrossRef Medline
12. Laird, D. W., Naus, C. C., and Lampe, P. D. (2017) SnapShot: connexins and disease. *Cell* **170,** 1260–1260.e1261 CrossRef Medline
13. Lutz, S. E., Zhao, Y., Gulinello, M., Lee, S. C., Raine, C. S., and Brosnan, C. F. (2009) Deletion of astrocyte connexins 43 and 30 leads to a dysmyelinating phenotype and hippocampal CA1 vacuolation. *J. Neurosci.* **29,** 7743–7752 CrossRef Medline
14. Ballard, C., Gauthier, S., Corbett, A., Brayne, C., Aarsland, D., and Jones, E. (2011) Alzheimer's disease. *Lancet* **377,** 1019–1031 CrossRef
15. Giaume, C., Saez, J. C., Song, W., Leybaert, L., and Naus, C. C. (2019) Connexins and pannexins in Alzheimer's disease. *Neurosci. Lett.* **695,** 100–105 CrossRef Medline
16. Selkoe, D. J., and Hardy, J. (2016) The amyloid hypothesis of Alzheimer's disease at 25 years. *EMBO Mol. Med.* **8,** 595–608 CrossRef Medline
17. De Strooper, B., and Karran, E. (2016) The cellular phase of Alzheimer's disease. *Cell* **164,** 603–615 CrossRef Medline
18. Querfurth, H. W., and LaFerla, F. M. (2010) Alzheimer's disease. *N. Engl. J. Med.* **362,** 329–344 CrossRef Medline
19. Mei, X., Ezan, P., Giaume, C., and Koulakoff, A. (2010) Astroglial connexin immunoreactivity is specifically altered at β-amyloid plaques in β-amyloid precursor protein/presenilin1 mice. *Neuroscience* **171,** 92–105 CrossRef Medline
20. Nagy, J. I., Li, W., Hertzberg, E. L., and Marotta, C. A. (1996) Elevated connexin43 immunoreactivity at sites of amyloid plaques in Alzheimer's disease. *Brain Res.* **717,** 173–178 CrossRef Medline
21. Yi, C., Mei, X., Ezan, P., Mato, S., Matias, I., Giaume, C., and Koulakoff, A. (2016) Astroglial connexin43 contributes to neuronal suffering in a mouse model of Alzheimer's disease. *Cell Death Differ.* **23,** 1691–1701 CrossRef Medline
22. Cruz, N. F., Ball, K. K., and Dienel, G. A. (2010) Astrocytic gap junctional communication is reduced in amyloid-β-treated cultured astrocytes, but not in Alzheimer's disease transgenic mice. *ASN Neuro* **2,** e00041 CrossRef Medline
23. Peters, O., Schipke, C. G., Philipps, A., Haas, B., Pannasch, U., Wang, L. P., Benedetti, B., Kingston, A. E., and Kettenmann, H. (2009) Astrocyte function is modified by Alzheimer's disease-like pathology in aged mice. *J. Alzheimer's Dis.* **18,** 177–189 CrossRef Medline
24. Orellana, J. A., Shoji, K. F., Abudara, V., Ezan, P., Amigou, E., Sáez, P. J., Jiang, J. X., Naus, C. C., Sáez, J. C., and Giaume, C. (2011) Amyloid β-induced death in neurons involves glial and neuronal hemichannels. *J. Neurosci.* **31,** 4962–4977 CrossRef Medline
25. Gajardo-Gómez, R., Labra, V. C., Maturana, C. J., Shoji, K. F., Santibanez, C. A., Saez, J. C., Giaume, C., and Orellana, J. A. (2017) Cannabinoids prevent the amyloid β-induced activation of astroglial hemichannels: a neuroprotective mechanism. *Glia* **65,** 122–137 CrossRef Medline
26. Yi, C., Ezan, P., Fernandez, P., Schmitt, J., Saez, J. C., Giaume, C., and Koulakoff, A. (2017) Inhibition of glial hemichannels by boldine treatment reduces neuronal suffering in a murine model of Alzheimer's disease. *Glia* **65,** 1607–1625 CrossRef Medline
27. Ren, R., Zhang, L., and Wang, M. (2018) Specific deletion connexin43 in astrocyte ameliorates cognitive dysfunction in APP/PS1 mice. *Life Sci.* **208,** 175–191 CrossRef Medline
28. Pike, C. J., Walencewicz-Wasserman, A. J., Kosmoski, J., Cribbs, D. H., Glabe, C. G., and Cotman, C. W. (1995) Structure-activity analyses of β-amyloid peptides: contributions of the β25-35 region to aggregation and neurotoxicity. *J. Neurochem.* **64,** 253–265 CrossRef Medline
29. Kubo, T., Nishimura, S., Kumagae, Y., and Kaneko, I. (2002) *In vivo* conversion of racemized β-amyloid ([D-Ser 26]Abeta1-40) to truncated and toxic fragments ([D-Ser 26]Abeta25-35/40) and fragment presence in the brains of Alzheimer's patients. *J. Neurosci. Res.* **70,** 474–483 CrossRef Medline
30. Gulyaeva, N. V., and Stepanichev, M. Y. (2010) Abeta(25-35) as proxyholder for amyloidogenic peptides: *in vivo* evidence. *Exp. Neurol.* **222,** 6–9 CrossRef Medline

31. Solan, J. L., and Lampe, P. D. (2009) Connexin43 phosphorylation: structural changes and biological effects. *Biochem. J.* **419,** 261–272 CrossRef Medline
32. Das Sarma, J., Wang, F., and Koval, M. (2002) Targeted gap junction protein constructs reveal connexin-specific differences in oligomerization. *J. Biol. Chem.* **277,** 20911–20918 CrossRef Medline
33. Musil, L. S., and Goodenough, D. A. (1991) Biochemical analysis of connexin43 intracellular transport, phosphorylation, and assembly into gap junctional plaques. *J. Cell Biol.* **115,** 1357–1374 CrossRef Medline
34. Berthoud, V. M., Minogue, P. J., Guo, J., Williamson, E. K., Xu, X., Ebihara, L., and Beyer, E. C. (2003) Loss of function and impaired degradation of a cataract-associated mutant connexin50. *Eur. J. Cell Biol.* **82,** 209–221 CrossRef Medline
35. Rubenstein, R. C., and Zeitlin, P. L. (2000) Sodium 4-phenylbutyrate downregulates Hsc70: implications for intracellular trafficking of ΔF508-CFTR. *Am. J. Physiol.* **278,** C259–C267 CrossRef
36. Das, S., Smith, T. D., Sarma, J. D., Ritzenthaler, J. D., Maza, J., Kaplan, B. E., Cunningham, L. A., Suaud, L., Hubbard, M. J., Rubenstein, R. C., and Koval, M. (2009) ERp29 restricts connexin43 oligomerization in the endoplasmic reticulum. *Mol. Biol. Cell* **20,** 2593–2604 CrossRef Medline
37. Chardin, P., and McCormick, F. (1999) Brefeldin A: the advantage of being uncompetitive. *Cell* **97,** 153–155 CrossRef Medline
38. Gumpert, A. M., Varco, J. S., Baker, S. M., Piehl, M., and Falk, M. M. (2008) Double-membrane gap junction internalization requires the clathrin-mediated endocytic machinery. *FEBS Lett.* **582,** 2887–2892 CrossRef Medline
39. Piehl, M., Lehmann, C., Gumpert, A., Denizot, J. P., Segretain, D., and Falk, M. M. (2007) Internalization of large double-membrane intercellular vesicles by a clathrin-dependent endocytic process. *Mol. Biol. Cell* **18,** 337–347 CrossRef Medline
40. De Bock, M., Decrock, E., Wang, N., Bol, M., Vinken, M., Bultynck, G., and Leybaert, L. (2014) The dual face of connexin-based astroglial Ca^{2+} communication: a key player in brain physiology and a prime target in pathology. *Biochim. Biophys. Acta* **1843,** 2211–2232 CrossRef Medline
41. Lauf, U., Giepmans, B. N., Lopez, P., Braconnot, S., Chen, S. C., and Falk, M. M. (2002) Dynamic trafficking and delivery of connexons to the plasma membrane and accretion to gap junctions in living cells. *Proc. Natl. Acad. Sci. U.S.A.* **99,** 10446–10451 CrossRef Medline
42. Musil, L. S., and Goodenough, D. A. (1993) Multisubunit assembly of an integral plasma membrane channel protein, gap junction connexin43, occurs after exit from the ER. *Cell* **74,** 1065–1077 CrossRef Medline
43. Wiley, J. C., Pettan-Brewer, C., and Ladiges, W. C. (2011) Phenylbutyric acid reduces amyloid plaques and rescues cognitive behavior in AD transgenic mice. *Aging Cell* **10,** 418–428 CrossRef Medline
44. Ricobaraza, A., Cuadrado-Tejedor, M., Marco, S., Perez-Otano, I., and Garcia-Osta, A. (2012) Phenylbutyrate rescues dendritic spine loss associated with memory deficits in a mouse model of Alzheimer disease. *Hippocampus* **22,** 1040–1050 CrossRef Medline
45. Ricobaraza, A., Cuadrado-Tejedor, M., Perez-Mediavilla, A., Frechilla, D., Del Rio, J., and Garcia-Osta, A. (2009) Phenylbutyrate ameliorates cognitive deficit and reduces tau pathology in an Alzheimer's disease mouse model. *Neuropsychopharmacology* **34,** 1721–1732 CrossRef Medline
46. Brusilow, S. W., and Maestri, N. E. (1996) Urea cycle disorders: diagnosis, pathophysiology, and therapy. *Adv. Pediatr.* **43,** 127–170 Medline
47. Fallon, R. F., and Goodenough, D. A. (1981) Five-hour half-life of mouse liver gap-junction protein. *J. Cell Biol.* **90,** 521–526 CrossRef Medline
48. Laird, D. W. (1996) The life cycle of a connexin: gap junction formation, removal, and degradation. *J. Bioenerg. Biomembr.* **28,** 311–318 CrossRef
49. Thomas, M. A., Zosso, N., Scerri, I., Demaurex, N., Chanson, M., and Staub, O. (2003) A tyrosine-based sorting signal is involved in connexin43 stability and gap junction turnover. *J. Cell Sci.* **116,** 2213–2222 CrossRef Medline
50. Bejarano, E., Girao, H., Yuste, A., Patel, B., Marques, C., Spray, D. C., Pereira, P., and Cuervo, A. M. (2012) Autophagy modulates dynamics of connexins at the plasma membrane in a ubiquitin-dependent manner. *Mol. Biol. Cell* **23,** 2156–2169 CrossRef Medline
51. Fong, J. T., Kells, R. M., Gumpert, A. M., Marzillier, J. Y., Davidson, M. W., and Falk, M. M. (2012) Internalized gap junctions are degraded by autophagy. *Autophagy* **8,** 794–811 CrossRef Medline
52. Jordan, K., Chodock, R., Hand, A. R., and Laird, D. W. (2001) The origin of annular junctions: a mechanism of gap junction internalization. *J. Cell Sci.* **114,** 763–773 Medline
53. Naus, C. C., Hearn, S., Zhu, D., Nicholson, B. J., and Shivers, R. R. (1993) Ultrastructural analysis of gap junctions in C6 glioma cells transfected with connexin43 cDNA. *Exp. Cell Res.* **206,** 72–84 CrossRef Medline
54. Leithe, E., Mesnil, M., and Aasen, T. (2018) The connexin 43 C-terminus: a tail of many tales. *Biochim. Biophys. Acta* **1860,** 48–64 CrossRef Medline
55. Basu, R., Banerjee, K., Bose, A., and Das Sarma, J. (2015) Mouse hepatitis virus infection remodels connexin43-mediated gap junction intercellular communication *in vitro* and *in vivo*. *J. Virol.* **90,** 2586–2599 CrossRef Medline
56. Schmittgen, T. D., and Livak, K. J. (2008) Analyzing real-time PCR data by the comparative C_T method. *Nat. Protocols* **3,** 1101–1108 CrossRef Medline
57. Schneider, C. A., Rasband, W. S., and Eliceiri, K. W. (2012) NIH Image to ImageJ: 25 years of image analysis. *Nat. Methods* **9,** 671–675 CrossRef Medline
58. Sali, A., and Blundell, T. L. (1993) Comparative protein modelling by satisfaction of spatial restraints. *J. Mol. Biol.* **234,** 779–815 CrossRef Medline
59. Shen, M. Y., and Sali, A. (2006) Statistical potential for assessment and prediction of protein structures. *Protein Sci.* **15,** 2507–2524 CrossRef Medline
60. D'Ursi, A. M., Armenante, M. R., Guerrini, R., Salvadori, S., Sorrentino, G., and Picone, D. (2004) Solution structure of amyloid β-peptide(25-35) in different media. *J. Med. Chem.* **47,** 4231–4238 CrossRef Medline
61. Jana, A. K., and Sengupta, N. (2015) Aβ self-association and adsorption on a hydrophobic nanosurface: competitive effects and the detection of small oligomers via electrical response. *Soft Matter* **11,** 269–279 CrossRef Medline
62. Menon, S., and Sengupta, N. (2017) Influence of hyperglycemic conditions on self-association of the Alzheimer's amyloid $\beta(A\beta_{1-42})$ peptide. *ACS Omega* **2,** 2134–2147 CrossRef Medline
63. Jana, A. K., and Sengupta, N. (2012) Adsorption mechanism and collapse propensities of the full-length, monomeric Aβ(1-42) on the surface of a single-walled carbon nanotube: a molecular dynamics simulation study. *Biophys. J.* **102,** 1889–1896 CrossRef Medline
64. Pierce, B. G., Wiehe, K., Hwang, H., Kim, B. H., Vreven, T., and Weng, Z. (2014) ZDOCK server: interactive docking prediction of protein-protein complexes and symmetric multimers. *Bioinformatics* **30,** 1771–1773 CrossRef Medline
65. Case, D. A., Betz, R. M., Cerutti, D. S., Cheatham, T. E., III, Darden, T. A., Duke, R. E., Giese, T. J., Gohlke, H., Goetz, A. W., Homeyer, N., Izadi, S., Janowski, P., Kaus, J., Kovalenko, A., Lee, T. S., *et al.* (2016) *Amber 16*, University of California, San Francisco
66. Maier, J. A., Martinez, C., Kasavajhala, K., Wickstrom, L., Hauser, K. E., and Simmerling, C. (2015) ff14SB: improving the accuracy of protein side chain and backbone parameters from ff99SB. *J. Chem. Theory Comput.* **11,** 3696–3713 CrossRef Medline
67. Onufriev, A., Bashford, D., and Case, D. A. (2004) Exploring protein native states and large-scale conformational changes with a modified generalized born model. *Proteins* **55,** 383–394 CrossRef Medline
68. Ryckaert, J.-P., Ciccotti, G., and Berendsen, H. J. C. (1977) Numerical integration of the cartesian equations of motion of a system with constraints: molecular dynamics of *n*-alkanes. *J. Comput. Phys.* **23,** 327–341 CrossRef
69. Phillips, J. C., Braun, R., Wang, W., Gumbart, J., Tajkhorshid, E., Villa, E., Chipot, C., Skeel, R. D., Kale, L., and Schulten, K. (2005) Scalable molecular dynamics with NAMD. *J. Comput. Chem.* **26,** 1781–1802 CrossRef Medline